Comparative Analysis of Large Eddy Simulation Models and Sensitivity Study for Turbulent Flow over a Backward-Facing Step

Nuttapong Khiaonoi[1], Punyawan Lumpaopong[1,*], Kwanchai Kraitong[1] and Jarupa Viyoch[2]

[1]Department of Mechanical Engineering, Faculty of Engineering, Naresuan University, Phitsanulok, 65000

[2]Department of Pharmaceutical Technology, Faculty of Pharmaceutical Sciences, Naresuan University, Phitsanulok, 65000

*Corresponding author. E-mail: punyawanl@nu.ac.th.

Abstract

The objective of this study is to compare three Large Eddy Simulation (LES) models: the k-equation, dynamic k-equation, and Wall-adaptive local eddy-viscosity (WALE) applied for simulating incompressible flow over a backward-facing step (BFS) using OpenFOAM®. The aim is to provide guidance for modeling complex turbulent flows using these LES models. The simulations replicated the experiment conducted by Driver and Seegmiller (1986), which applied the inlet flow at the Reynolds number of 36,000 and exited at atmospheric pressure. All walls were treated as non-slip surfaces. The models were evaluated based on their accuracy compared with experimental data, computational cost, and stability. The results showed that, the k-equation model had the highest accuracy, aligning closely with the experimental results. However, this level of performance caused higher computational cost in comparison to the dynamic k-equation and WALE models. The subsequent study involved varying the mesh size of the k-equation model from 30,000 to 100,000 cells and the time step from 5×10^{-5} to 5×10^{-4} seconds to examine the sensitivity of these parameters on the model's performance. The numerical results from the various models showed that the k-equation model with 70,000 cells and a time step of 5×10^{-4} seconds provided the optimal performance. These findings provide a practical framework for selecting and applying LES models in complex turbulent flows, improving both reliability and efficiency in LES simulations.

Keywords: Large Eddy Simulation, K-equation model, Backward-Facing Step Flow, OpenFOAM

Introduction

Computational Fluid Dynamics (CFD) has become a fundamental numerical simulation tool in engineering and scientific research over decades because of its ability to facilitate the modeling and simulation of complex flow phenomena in aerospace, automotive, and biomedical engineering (Morrison et al., 2017; Nielsen & Diskin, 2017; Rahimi-Gorji et al., 2022; Shukla et al., 2025). The most challenging task in CFD is turbulence flow simulations dealing with the effects of chaotic three-dimensional fluctuations of velocity and pressure.

Turbulence or instability flow occurs when the transfer of momentum, mass and energy forms a wide range of multi-scale swirling fluid motions or eddies. To capture them accurately, substantial computational resource is needed. However, it often becomes a limitation in industrial applications due to cost and time constraints. The conventional turbulence modelling approaches are 1) Reynolds-Averaged Navier-Stokes (RANS) 2) Direct Numerical Simulation (DNS) and 3) Large Eddy Simulation (LES). The RANS approach offers computational efficiency by averaging the effects of turbulence. However, it lacks ability to capture unsteady and anisotropic flow behavior accurately (Park et al., 2021). Meanwhile, the DNS resolves all scales of turbulence with high resolution (Luo, 2019; Moin & Mahesh, 1998) but extremely high computational cost and resource requirements are its drawbacks. The LES positions between the two approaches. Instead of resolving all scales of turbulence, it focuses on capturing only the dominant flow structures responsible for most of the energy transfer, therefore, significantly reduces computational demands while preserving the essential features of complex turbulent flows (Pope, 2000). The backward-facing step (BFS) is a conventional benchmark geometry for visualizing turbulence flows, sharp separation, reattachment, and complex shear-layer dynamics (Avancha & Pletcher, 2002; Singh et al., 2020). Previous studies have compared LES models based on algebraic equations, such as the Smagorinsky and Wall-adaptive local eddy-viscosity (WALE) models, to assess their influence on flows in the near-wall region (Akselvoll & Moin, 1993; Arya & De, 2021; Shehadi, 2018). Many researchers have studied LES models based on transport equations such as the k-equation model. They have simulated and validated with the BFS flow to examine the performance of capturing mean flow characteristics and turbulence intensities (Keating et al., 2004; Panjwani et al., 2012; Shehadi, 2018). However, all of the studies have not yet considered the effects of model adaptation, mesh resolution, time step sensitivity. Moreover, the near-wall behaviors of the turbulent flow simulation remains unclear. Therefore, the objective of this study was to offer a comprehensive evaluation framework and practical guidance for the effective selection of LES models in complex turbulent flows, thereby contributing to enhanced reliability and efficiency in future LES applications.

Materials and Methods

Computational Fluid Dynamics (CFD)

The governing equations of CFD consist of the conservation of mass and momentum expressed in the list of equations below (Moukalled et al., 2016).

Conservation of mass (Continuity equation):

$$\frac{\partial \rho}{\partial t} + \nabla \cdot (\rho \mathbf{u}) = 0 \qquad (1)$$

Conservation of momentum (Navier-Stokes equation):

$$\frac{\partial}{\partial t}[\rho \mathbf{u}] + \nabla \cdot \{\rho \mathbf{u}\mathbf{u}\} = -\nabla p + \mu \nabla^2 \mathbf{u} + F \qquad (2)$$

when:

$\mathbf{u}$	=	the velocity vector (m/s)	t	=	time (s)
ρ	=	density (kg/m^3)	F	=	external forces (N)

Large eddy simulation (LES)

In LES, the large eddies are calculated directly by the numerical method while small eddies are filtered out. The small unresolved motions are called the Sub-grid Scale (SGS) (Pope, 2000). The sizes of eddies are defined by their length scale (ℓ), which corresponds to the turbulent kinetic energy (k), and can be written as shown in equation (5).

$$\ell = \frac{k^{3/2}}{\varepsilon} \tag{5}$$

when: ℓ = eddy length scale (m) k = turbulent kinetic energy (J) ε = specific heat (J/kg.K)

A filter is applied to the velocity field across the grid size, smoothing the flow at smaller scales and capturing only the larger motions. The general filter velocity equation is shown in equation (6)

$$\bar{\phi}(\mathbf{x}, t) = \int_{\Omega} G(\mathbf{x}-\mathbf{r})\phi(\mathbf{r}, t)dr \tag{6}$$

when:

$\bar{\phi}(\mathbf{x}, t)$	=	filtered field at position x and time t	$G(\mathbf{x}-\mathbf{r})$	=	filter kernel
$\phi(\mathbf{r}, t)$	=	filtered field at position r and time t	Ω	=	domain of integration

After filtering, the governing equation of momentum conservation in equation (2) became:

$$\frac{\partial \bar{\mathbf{u}}}{\partial t} + \left(\bar{\mathbf{u}} \cdot \nabla\right)\bar{\mathbf{u}} = \nu\nabla^2\bar{\mathbf{u}} - \left(\frac{1}{\rho}\nabla\bar{p} + \nabla \cdot \tau^{SGS}\right) + F \tag{7}$$

when :

τ^{SGS}	=	subgrid-scale stress (m^2/s^2)	$\bar{\mathbf{u}}$	=	filtered velocity vector (m/s)

There are many different models to approximate the apparent stress tensor that appears in the governing equations as a consequence of the filtering operation. This study focuses on the WALE, k-equation and dynamic k-equation models. The WALE model has been developed based on the Smagorinsky framework to allows the model to automatically adapt to the flow without relying on any fixed coefficients (Shehadi, 2018), by taking into account the effects of swirling and rotational flows alongside the strain rate. In WALE, the stress tensor of the SGS model adheres to equation (8).

$$\tau_{ij}^{SGS} - \frac{1}{3}\tau_{kk}^{SGS}\delta_{ij} = -2\left((C_w\Delta)^2 \frac{(S_{ij}^d S_{ij}^d)^{3/2}}{(\bar{S}_{ij}\bar{S}_{ij})^{3/2} + (S_{ij}^d S_{ij}^d)^{5/4}}\right)\left(\frac{1}{2}\left(\frac{\partial \bar{u}_i}{x_j} + \frac{\partial \bar{u}_j}{x_i}\right)\right) \tag{8}$$

when:

τ_{ij}^{SGS}	=	subgrid-scale (SGS) stress tensor (Pa)	S_{ij}	=	mean strain rate tensor (1/s)	δ_{ij}	=	Kronecker
τ_{kk}^{SGS}	=	trace of the SGS stress tensor (Pa)	$\bar{S}_{ij}$	=	filtered stain tensor (1/s)	Δ	=	filter width (m)
ν_t	=	turbulent kinematic viscosity (m^2/s)	S_{ij}^d	=	rotational rate tensor ($1/s^2$)	C_w	=	0.325

The Smagorinsky and WALE models determine sub-grid viscosity through local velocity gradients without solving any time-dependent equations for turbulence evolution. Therefore, the approaches may neglect significant temporal variations and flow separations in turbulence intensity when the turbulence is not in equilibrium (Gao et al., 2019). The temporal variations of flow in non-equilibrium turbulence can be achieved by applying a transport equation for SGS turbulent kinetic energy, which accounts for the generation, transport, and dissipation of turbulence energy throughout the flow domain. The commonly used LES models that employs this transport equation is the k-equation model (Panjwani et al., 2012), in which the stress tensor is modelled by

$$\tau_{ij}^{SGS} - \frac{2}{3}\tau_{kk}^{SGS}\delta_{ij} = -2\nu_{sgs}S_{ij} \tag{9}$$

when: $\nu_{sgs} = C_k\sqrt{k_{sgs}}\Delta$

The transport equation for the SGS kinetic energy (k_{sgs}) can be written as:

$$\frac{\partial k_{sgs}}{\partial t} + \bar{u}_j\frac{\partial k_{sgs}}{\partial x_j} = 2\nu_{sgs}\bar{S}_{ij}\bar{S}_{ij} - C_\varepsilon\frac{k_{sgs}^{3/2}}{\Delta} + \frac{\partial}{\partial x_j}\left(\frac{\nu_{sgs}}{\sigma_k}\frac{\partial k_{sgs}}{\partial x_j}\right) \tag{10}$$

where:

ν_{sgs}	=	Subgrid-scale kinetic energy (m^2/s)	C_k	=	empirical model coefficients
k_{sgs}	=	trace of the SGS stress tensor (m^2/s^2)	C_ε	=	empirical model coefficients

The k-equation model is a more realistic and dynamic estimation of eddy viscosity, improving accuracy in flows with strong non-equilibrium effects. The model relies on empirically determined model coefficients, which may not generalize well across different flow types. The dynamic k-equation model is developed by enhancing the framework through the automatic adjustment of model coefficients based on local flow conditions and utilizing velocity filtering to improve its capacity to capture flow variation (Shehadi, 2018). The algorithm to adjust the model coefficient is as follows.

$$C_k = \frac{L_{ij}M_{ij}}{M_{kl}M_{kl}} \tag{11}$$

where:

L_{ij}	=	difference of test-filtered resolved stresses (Pa)
M_{ij}	=	difference between modeled test-level and grid-level SGS stresses (Pa)
$M_{kl}M_{kl}$	=	Norm squared of $M_{ij}M_{ij}$ used to normalize in least-squares solution (Pa^2)

CFD Modeling and Simulation

BSF Geometry model

In Figure 1, the step of the BFS model is located at x=0, serving as the reference point. The inlet height measures 10.2 cm, and the upstream distance from the inlet is 165 cm to ensure fully developed flow before entering the step. The circulation zone, ranging from P2 to P5, is located between x/H = 1 and x/H = 6.

The recovery point, where the flow is expected to reattach and redevelop along the pipe, is located at P5. The downstream location (P6) is 12.7 cm away from the step.

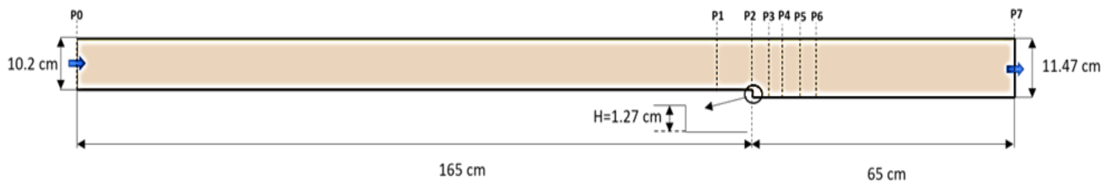

Figure 1 Geometry of the backward-facing step

Mesh Model

For the baseline simulations, the geometry of the BSF was divided into five zones, each of which was assigned with a different mesh (computational grid) density as shown in Figure 2, based on the anticipated flow characteristics. The cell size varies depending on the location within the flow domain. The region between the entrance and the upstream position had a medium mesh density to precisely represent the fully developed inflow. The recirculating zone had the highest mesh density to precisely resolve flow separation and capture flow fluctuations. The number of cells in total was 50,000 cells.

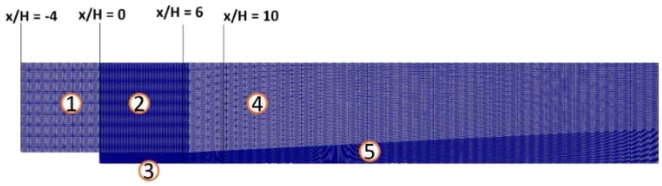

Figure 2 Computational grid density zones: (1) Upstream zone (2) Recirculation zone (3) Near wall 1- inside the recirculation zone (4) Recovery zone and (5) Near wall 2 - inside the recovery zone.

Boundary conditions

The inlet flow velocity (U_{inlet}) of the air flow was 44.2 m/s, corresponding to a Reynolds number (Re) of 3600. The step position was designated as x/H=0, with the upstream position at x/H= -4, when the flow was presumed to be fully developed. Velocity profile measurements are obtained at the following positions: x/H = -4, 0, 4, 6, and 10, respectively. The wall boundaries were set to no slip and the outlet condition was the atmospheric pressure.

Model Simulations

This study used OpenFOAM® v2412 to simulate the BFS flow, replicating the research conducted by Driver and Seegmiller (1982). The simulations were carried out by adjusting the mesh resolution and time-step size. The simulations are executed using (LES) with a maximum Courant number (Co) of 5, ensuring stability and an appropriate level of accuracy. Additionally, the wall distance (y+) is maintained below 1.5, which is essential for accurately resolving near-wall turbulence. The formulas for the Courant number and wall distance are presented below.

$$Co = |u| \frac{\Delta x}{\Delta t} \tag{12}$$

$$y^{+} = \frac{y\tau}{\nu} \tag{13}$$

where: τ = the wall shear stress (Pa) y= distance from the wall (m) ν = kinematic viscosity (m^2/s)

The LES baseline simulations were performed to study the three SGS models: k-equation, dynamic k-equation and WALE, using a time step of 5×10^{-5} seconds. The simulation results were compared with velocity profiles and recirculation zone behaviour obtained from the experimental data of Driver and Seegmiller (1982). The most accurate LES model were selected to further study using various mesh resolutions and time-steps, both of which are crucial in terms of CFD simulation, to investigate model's sensitivity, robustness, and the trade-off between accuracy and computational cost. The summary of the numerical procedure is shown in Table 1. Simulation results were compared using relative error expressed as a ratio of the absolute difference to the experimental value.

Table 1 Simulation study conditions

Simulation	SGS Model	Mesh configuration	Number of cells	Time-step
Baseline	k-equation dynamics k-equation WALE	M2	50,000	5 x 10^{-4} s
Mesh study	selected baseline model	M1	30,000	5 x 10^{-4} s
		M2	50,000	
		M3	70,000	
		M4	100,000	
Time-step study	selected baseline model	M1	30,000	5 x 10^{-4} s 1 x 10^{-4} s 5 x 10^{-5} s

Results

Streamlines and velocity profiles obtained from the baseline simulations are shown in Figures 3 and 4. The k-equation and WALE models produced streamlines with reattachment points at about x/h=6, which was close to the experimental value of 6.26. The dynamic k-equation model shows two reattachment points at x/h = 6 and 10. The numerical instability in the dynamic k-equation model may explain the increased separation and unsteady behavior beyond x/h=10.

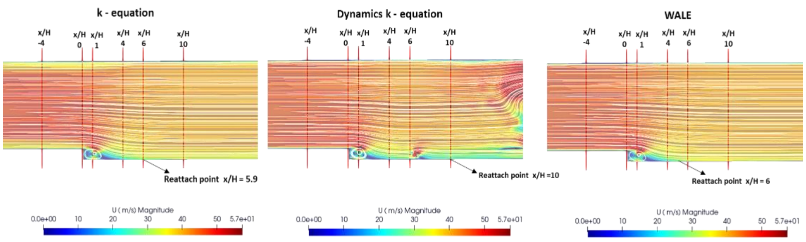

Figure 3. The velocity field of LES models.

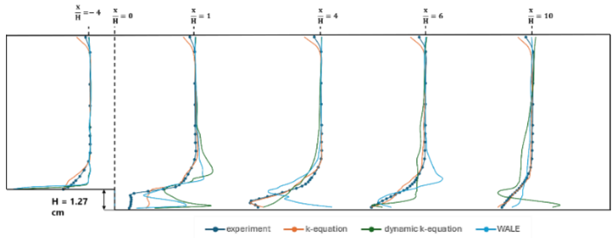

Figure 4. Velocity profile comparison between LES models and experimental data.

Figure 4 reveals that the k-equation model matched the experimental data the most, meanwhile, the WALE model performs worse than the dynamic k-equation model in the recirculating zone (x/h = -4 to 10). The WALE model velocity profiles were more accurate at x/h=4 and x/h=10 when the flow was more stable. Table 2 shows the relative error from x/h = -4 to 10. Among the three models, the k-equation had the lowest relative error. The k-equation model had a relative error of 1.963 at x/h=1, an area with vital flow fluctuations near the step and performed well in the recirculation zone with relative errors between 0.049 and 0.081.

Table 2. Relative velocity error of LES models

Location	Relative Error							
	k-equation						dynamic k-equation	WALE
	M1			M2	M3	M4	M2	
	T1	T2	T3	T1				
x/h =-4	0.0300	0.0326	0.0363	0.042	0.0360	0.041	0.0890	0.133
x/h = 1	0.105	0.8616	0.5092	1.963	0.0680	0.075	5.003	2.958
x/h = 4	0.063	0.0434	0.0452	0.081	0.0460	0.042	0.212	0.194
x/h = 6	0.082	0.0812	0.0647	0.049	0.0520	0.039	0.309	0.122

Table 3 presents the summary of the computational cost, stability, and convergence associated with the LES models. The k-equation model had the lowest y+ and Courant number, suggesting enhanced stability. However, it required additional 20-30 minutes of computation time compared to the WALE and dynamic k-equation models. The residual differences among the models were not significant.

Table 3. Summary of LES model performance

Parameter	Performance							
	k-equation						dynamic k-equation	WALE
	M1			M2	M3	M4	M2	
	T1	T2	T3	T1				
Computation time (s)	3,987	19,270	32,340	5,276	5,577	5,276	3,478	4,096
RAM(GB)	6.3	6.3	6.1	6.3	6.4	6.3	6.3	6.3
Courant number	2.73	0.56	0.29	3.71	4.26	3.71	4.12	3.86
y+	0.23	0.68	0.69	0.46	0.17	0.46	1.27	1
residual of velocity	6.6E-09	6.56E-09	9.52E-09	9.97E-09	5.26E-09	4.80E-09	9.66E-09	8.62E-09
residual of pressure	9.99E-07	9.92E-07	9.99E-07	9.9E-07	9.91E-07	9.94E-07	8.62E-07	8.62E-07

The k-equation model was then chosen for further investigation on mesh resolution and time-step sensitivity. It was found that the overall flow patterns of the velocity fields and streamlines corresponding to mesh configurations M1 through M4 appeared to be similar. The velocity profiles of the k-equation model for all mesh configurations agreed well with the experimental data (Figure 5)

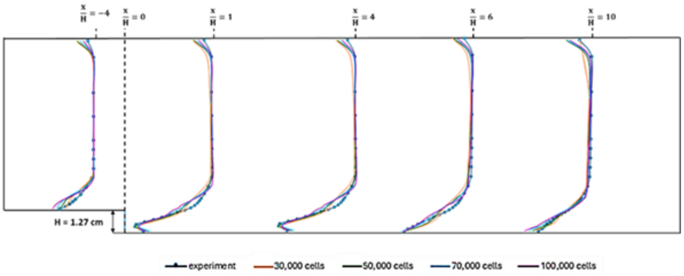

Figure 5 Velocity profiles of the k-equation model comparison between mesh configuration

Table 2 also shows that the configurations M2 and M3, with total cell counts of 50,000 and 70,000, respectively, resulted in higher accuracy. M3 provided the optimal balance of accuracy and stability, with the lowest y+ value of 0.17. A subsequent numerical experiment varied the time-step (T) using the coarser mesh configuration, M1 (30,000 cells), to evaluate the effects of time-step on the accuracy and performance of the k-equation model. Figure 6 shows that as the time step decreased, the finer vortical structures near the step region were captured. Figure 7. compared the velocity profiles with experimental data at x/h = -4, 6, and 10, showing strong overall agreement.

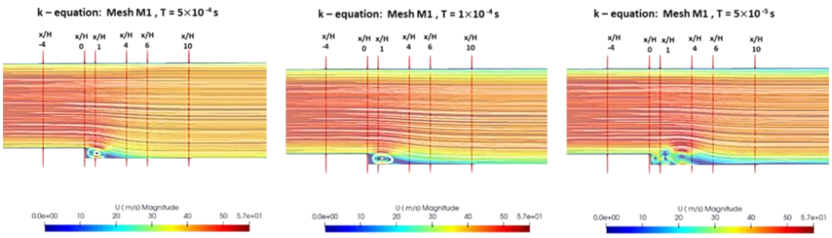

Figure 6. The velocity field of k-equation models with various simulation time-step.

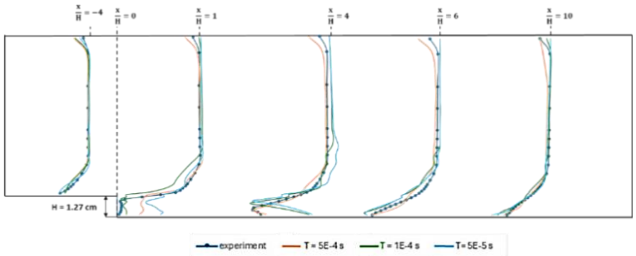

Figure 7. Velocity profile of the k-equation models with various simulation time-step.

The time step of 1×10^{-4} s for M1 case provided the highest accuracy (Table 2). However, the time step of 5×10^{-5} s achieved a better balance between accuracy and numerical stability, but required more computational time.

Discussion

The simulation results of the baseline SGS models Results agreed with previous studies (Keating et al., 2004; Panjwani et al., 2012; Shehadi, 2018). This study elaborated the work on the importance of turbulence of turbulence model selection, mesh resolution and time-step size for effective turbulent modeling with LES. Increasing mesh density improved flow detail resolution, but too fine meshes could reduce accuracy by overestimating vortices, especially when using improper time-step. The experimental results showed that the k-equation model with a mesh of 70,000 cells (M3) and a time step of 5×10^{-4} s achieved the best balance between accuracy and numerical stability. Decreasing the time-step enhanced numerical stability and provided higher precision for unsteady flow characteristics. However, smaller time-steps elevated computational expenses. A time-step of 5×10^{-4} s was determined to provide the optimal solution for accuracy, stability, and efficiency. The k-equation model provided the most precise velocity profiles and reattachment forecasts but required more computational time. The dynamic k-equation model performed simulations faster, however, showed instability in downstream areas due to an inequality between numerical setup, mesh density, and time step. The model effectively allowed complicated flow structures but was sensitive to numerical configuration.

Conclusions

This study evaluated three LES models: the k-equation, the dynamic k-equation, and the WALE model for simulating turbulent flow over a BFS. The k-equation model was the most accurate, particularly in predicting velocity profiles and reattachment points, with optimal performance achieved using a mesh of 70,000 cells and a time step of 5×10^{-4} seconds. The dynamic k-equation was computationally efficient, but showed instability due to its sensitivity to mesh and time-step settings. In contrast, the WALE model provided good stability in low fluctuation regions. By comparing accuracy, stability, and computational cost, this study successfully achieved its objective of providing a practical framework for selecting LES models. These findings could be applied as a guidance when analyzing complex turbulent flow. Future work should focus on optimized numerical settings and adaptive mesh and time-step strategies to improve the accuracy and efficiency of the LES.

Acknowledgement

I sincerely thank the Faculty of Engineering, Naresuan University, for awarding me the doctoral scholarship in 2022 and supporting me throughout my Ph.D. studies. This support allowed me to focus fully on my research and greatly contributed to my academic and professional development.

References

Akselvoll, K., & Moin, P. (1993). Large eddy simulation of a backward facing step flow. In *Engineering turbulence modelling and experiments* (pp. 303–313). Elsevier. https://doi.org/10.1016/B978-0-444-89802-9.50033-2

Avancha, R. V. R., & Pletcher, R. H. (2002). Large eddy simulation of the turbulent flow past a backward-facing step with heat transfer and property variations. *International Journal of Heat and Fluid Flow*, *23*, 601–614.

Driver, D. M., & Seegmiller, H. L. (1985). Features of a reattaching turbulent shear layer in divergent channel flow. *AIAA Journal*, *23*(2), 163–171.

Gao, W., Zhang, W., Cheng, W., & Samtaney, R. (2019). Wall-modelled large-eddy simulation of turbulent flow past airfoils. *Journal of Fluid Mechanics*, *873*, 174–210.

Keating, A., Piomelli, U., Bremhorst, K., & Nešić, S. (2004). Large-eddy simulation of heat transfer downstream of a backward-facing step. *Journal of Turbulence*, *5*(1), 020.

Luo, D. (2019). Numerical simulation of turbulent flow over a backward facing step using partially averaged Navier-Stokes method. *Journal of Mechanical Science and Technology*, *33*(5), 2137–2148.

Moin, P., & Mahesh, K. (1998). Direct numerical simulation: a tool in turbulence research. *Annual review of fluid mechanics*, *30*(1), 539–578.

Morrison, T. M., Dreher, M. L., Nagaraja, S., Angelone, L. M., & Kainz, W. (2017). The role of computational modeling and simulation in the total product life cycle of peripheral vascular devices. *Journal of medical devices*, *11*(2), 024503.

Moukalled, F. H., Mangani, L., & Darwish, M. (2016). *The Finite Volume Method in Computational Fluid Dynamics (Stuttgart, Germany)*. Springer.

Nielsen, E. J., & Diskin, B. (2017). High-performance aerodynamic computations for aerospace applications. *Parallel Computing*, *64*, 20-32.

Panjwani, B., Ertesvåg, I. S., Gruber, A., & Rian, K. E. (2012). Large eddy simulation in generalized curvilinear coordinates using conventional approach: Theory and validation. *International Journal for Numerical Methods in Fluids*, *69*(3), 671–690.

Park, J., Ha, S., & You, D. (2021). On the unsteady Reynolds-averaged Navier–Stokes capability of simulating turbulent boundary layers under unsteady adverse pressure gradients. *Physics of Fluids*, *33*(6), 65125.

Pope, S. B. (2000). *Turbulent Flows* (1st ed.). Cambridge.

Rahimi-Gorji, M., Debbaut, C., Ghorbaniasl, G., Cosyns, S., Willaert, W., & Ceelen, W. (2022). Optimization of intraperitoneal aerosolized drug delivery using computational fluid dynamics (CFD) modeling. *Scientific Reports*, *12*(1), 6305.

Shehadi, E. (2018). *Large eddy simulation of turbulent flow over a backward-facing step* [Master's thesis]. Uppsala University.

Shukla, P. K., Mishra, R., & Tewari, R. P. (2025). CFD Analysis of Straightener Designs on Overall Performance of the Axial Flow Blood Pump. *Journal of Applied Fluid Mechanics*, *18*(2), 304-316.

Singh, A., Aravind, S., Srinadhi, K., & Kannan, B. T. (2020, August). Assessment of turbulence models on a backward facing step flow using OpenFOAM®. In *IOP Conference Series: Materials Science and Engineering* (Vol. 912, No. 4, p. 042060). IOP Publishing. https://doi.org/10.1088/1757-899X/912/4/042060